Atmospheric Research 220 (2019) 1–9

Contents lists available at ScienceDirect

Atmospheric Research

journal homepage: www.elsevier.com/locate/atmosres

Mass size distribution of major monosaccharide anhydrides and mass contribution of biomass burning

Zoltán Imre Blumberger[a], Anikó Vasanits-Zsigrai[a], Gergő Farkas[a,b], Imre Salma[a,*]

[a] Institute of Chemistry, Eötvös University, H-1518 Budapest, P.O. Box 32, Hungary
[b] Air Quality Reference Center, Hungarian Meteorological Service, H-1181 Budapest, Gilice tér 39, Hungary

ARTICLE INFO

Keywords:
Levoglucosan
Mannosan
Galactosan
Molecular marker
MOUDI
Wood burning

ABSTRACT

Aerosol samples were collected by a MOUDI cascade impactor in central Budapest in winter 2017, and were analysed by GC–MS and AAS methods for major monosaccharide anhydrides, i.e. levoglucosan (LVG), mannosan (MAN) and galactosan (GAN), and for K, which are important chemical markers for biomass burning (BB) emissions. Their median atmospheric concentrations were 0.36 μg m^{-3}, 37 ng m^{-3}, 10.9 ng m^{-3} and 0.32 μg m^{-3}, respectively. Detailed mass size distributions were determined in an aerodynamic diameter range of 0.053–9.9 μm for all markers. There were 3 modes identified in the distributions of the monosaccharide anhydrides with typical mass median aerodynamic diameters (MMADs) and relative modal concentrations (RMCs) of 0.42 μm and 90%, 1.62 μm and up to 9%, and 0.11 μm and up to 9%, respectively. The modes were assigned to the condensation and droplet submodes (formed by splitting) of a dominant accumulation mode and to a minor accumulation mode, respectively. The former 2 modes were generated by BB, while the latter mode was explained by another source type with higher burning temperature than BB, which is likely lignite combustion. The size distributions of K also contained 3 modes with mean MMADs and RMCs of 0.40 μm and 78%, 0.16 μm and 12%, and 5.8 μm and 10%, respectively. The former 2 modes were assigned to a major and a minor accumulation mode similarly to the monosaccharide anhydrides, while the latter peak is a coarse mode. Levoglucosan was further utilised to estimate the PM_{10} mass originating from BB, which yielded a mean relative contribution of 18%. This implies that BB represents a considerable or substantial source for particulate mass in the area. Concentration ratios among the monosaccharide anhydrides suggested that it is the wood burning that is the major form of BB, and that the relative share of softwood burnt to hardwood is around 46%.

1. Introduction

Biomass burning (BB) includes wildfires, intentional agricultural fires and burning of wood, straw, grain, bio-oils and organic waste in household appliances for heating, cooking or pleasure, in boilers and industrial power plants. The latter forms have an increasing role in decentralised and substitute energy production (Vicente and Alves, 2018). Biomass burning is an important source type for particulate matter (PM), carbonaceous aerosol particles (Saarikoski et al., 2007; Szidat et al., 2009; Claeys et al., 2010; Gilardoni et al., 2011; Saarnio et al., 2012; Herich et al., 2014; Chen et al., 2017; del Águila et al., 2018) and some further compounds of special interest such as polycyclic aromatic hydrocarbons (PAHs; e.g. Hays et al., 2003). It can yield enlarged atmospheric concentrations on seasonal time scale or as a tendency. Disadvantages and potential risks related to BB have been increasingly recognised. Smoke from BB can affect regional or local visibility, air quality, ecosystems, built environment, cloud processes, climate and human health (e.g. Chen et al., 2017 and references therein). Quantification of the contributions from BB to various aerosol species is necessary to better understand its relevance, role and effects. There are several receptor models, which facilitate its quantification on the basis of atmospheric concentrations and some properties which are derived from theoretical models (e.g. wavelength dependence of optical absorption coefficient; e.g. Favez et al., 2010 and references therein). They primarily include: 1) single marker methods, which are mainly based on molecular tracers (see below) or ^{14}C (e.g. Szidat et al., 2006; Minguillón et al., 2011; Zhang et al., 2012; Bernardoni et al., 2013, and references therein) or their combination (Salma et al., 2017), 2) the so-called Aethalometer model and its developed versions (e.g. Sandradewi et al., 2008a, 2008b; Zotter et al., 2017 and references therein) and 3) multivariate statistical receptor models (e.g. Hopke, 2016 and references therein; Maenhaut et al., 2016). The marker methods are

* Corresponding author.
E-mail address: salma@chem.elte.hu (I. Salma).

https://doi.org/10.1016/j.atmosres.2019.01.001
Received 12 September 2018; Received in revised form 14 December 2018; Accepted 2 January 2019
Available online 07 January 2019
0169-8095/ © 2019 Elsevier B.V. All rights reserved.

advantageous from the point of view that they do not require many samples or extensive and complex data sets, are quite straightforward, and, therefore, they are often the choice for source apportionment studies.

During pyrolysis of cellulose- and hemicellulose-containing bulk material, 3 stereoisomers of a monosaccharide anhydride of $C_6H_{10}O_5$, namely levoglucosan (LVG, 1,6-anhydro-β-D-glucopyranose, Simoneit et al., 1999), mannosan (MAN, 1,6-anhydro-β-D-mannopyranose) and galactosan (GAN, 1,6-anhydro-β-D-galactopyranose; Nolte et al., 2001) are formed in relatively large concentrations (Locker, 1988; Simoneit et al., 1999). They are initially generated as gaseous molecules at temperatures larger than 300 °C, and subsequently condense onto pre-existing particles due to their low vapour pressure as the temperature decreases (Caseiro et al., 2009). Levoglucosan is the most abundant of them (e.g. Table 2) and it is reasonably stable in the atmosphere towards photolysis and acid-catalysed hydrolysis (Locker, 1988; Fraser and Lakshmanan, 2000; Simoneit et al., 2004). Its atmospheric lifetime of 10 d can be decreased by chemical reactions with OH radical in the aqueous phase under high relative humidities (RHs, Hennigan et al., 2010; Hoffmann et al., 2010). Such conditions can be important in tropical areas or for aged (long-range transported) smoke plumes in summer. Nevertheless, LVG was found to be a suitable molecular marker in many studies (e.g. Simoneit et al., 1999; Zdráhal et al., 2002; Puxbaum et al., 2007; Saarikoski et al., 2008; Szidat et al., 2009; Maenhaut et al., 2012, 2016; Yttri et al., 2014). Levoglucosan can also be produced in lignite (Fabbri et al., 2009) and peat combustion (Iinuma et al., 2007; Fabbri et al., 2008; Kourtchev et al., 2011), although their contributions are usually neglected. The relationships among the stereoisomers can also provide information on the ratios of hardwood and softwood burning. The determination of the monosaccharide anhydrides in aerosol samples is well established by now, and can be performed by various analytical methods (Yttri et al., 2015). Some inorganic species such as K are also produced in large abundances by BB (e.g. Maenhaut et al., 1996, 2016; Chen et al., 2017), although it also has further substantial sources such as sea spray, meat cooking or refuse incinerators (e.g. Zhang et al., 2014). The measurement of the corresponding water-soluble (non-sea salt) K in aerosol samples can be commonly realised by various standard analytical methods. It has to be notes that BB also produces a large variety of PAHs, which have distinctive relevance for human health (Hays et al., 2003 and references therein). Their measurements and particularly their collections requires special considerations to avoid the loss of PAHs from the substrates or filters (Hays et al., 2003).

Particulate matter from BB is expected to occur in fine size fraction due to high-temperature emissions or condensation processes of corresponding vapours. Since the burning temperatures can differ for various biomass types (e.g. lignite, wood or straw), it is expected that the temperatures can have implications on the size distributions of primary BB products, including its major molecular markers. The size distributions can further be modified by transformation (e.g. dissolution of gases, multiphase chemical reactions, water activation, condensation of vapours, coagulation in the aerosol population or aging) processes during atmospheric transport under varying meteorological, chemical and physical conditions. Such (small) differences in the shape of the distributions associated with the transformation processes or similar source types can be investigated by utilising an increased size resolution of modern cascade impactors (with larger number of stages, e.g. Marple et al., 1991), some developments in their calibration and advanced mathematical algorithms for processing their experimental data (Wolfenbarger and Seinfeld, 1990), which became available recently (see Section 2.3.). The perspective results can have relevance mainly for refining the source apportionment methods based specifically on monosaccharide anhydrides from BB.

In earlier aerosol studies in Budapest, atmospheric concentrations, contributions and mass size distributions of several relevant carbonaceous chemical species were determined (e.g. Salma et al., 2004, 2007, 2013; Claeys et al., 2012), and source apportionment of major carbonaceous species to fossil fuel (FF) combustion, BB and biogenic emissions was realised by a coupled radiocarbon-levoglucosan marker method (Salma et al., 2017). Size distributions of carbonaceous molecular markers of BB (namely LVG and its stereoisomers) and related important information have been missing internationally. The objectives of this research are to determine and present detailed mass size distributions of major monosaccharide anhydrides by using a cascade impactor sampler and an advanced inversion algorithm, to relate their fine structure to possible source types and atmospheric transformation processes, to quantify the relative importance of the processes identified, to discuss the consequences of the modal structure on the LVG marker method, and to estimate also the contribution of BB to PM_{10} mass and relative ratios of hardwood and softwood burning. The results and conclusions are based on aerosol samples collected in winter, when the emissions, concentrations and contributions from BB are expected to be the largest.

2. Methods

2.1. Aerosol sampling and on-line measurements

The aerosol samples were collected at the Budapest platform for Aerosol Research and Training (BpART) facility situated near the river Danube (N 47° 28′ 29.9″, E 19° 3′ 44.6″, 115 m above mean see level, Salma et al., 2016). The site represents a well-mixed, average atmospheric environment for the city centre thank to orographic, physical and typical meteorological conditions around the location (Salma et al., 2016). The collection campaign took place continuously from 07:00 on Sunday, 24–12–2017 to 07:10 on Saturday, 30–12–2017. Local time (LT = UTC + 1) was chosen as the time base because the daily activity time pattern of inhabitants substantially influences the atmospheric concentrations in cities (Salma et al., 2014). There was no wildfire in the larger area in this time interval. A microorifice uniform deposit impactor (MOUDI, type 110, Marple et al., 1991) was deployed with a simple rain shield. The sampler has 11 impaction stages labelled from 0 to 10 with 50% cut-off aerodynamic diameters of d_{50} = 18, 9.9, 6.2, 3.1, 1.8, 1.0, 0.603, 0.301, 0.164, 0.094 and 0.053 μm, respectively. The stage 0 was utilised as upper size cut-off inlet. The samples were collected on 47-mm diameter ungreased polycarbonate membrane filters (with a pore size of 0.4 μm). The cascade impactor operated at an air flow rate of 30 L min^{-1}. The collection efficiency curves for the impaction stages of the MOUDI were supplied by the manufacturer, and they were fine-tuned according to their experimentally determined 50% cut-off values. A total of 4 aerosol sample sets were obtained together with 1 set of field blanks. The first (S1) and last (S4) sample sets were collected for 48 h, while the other 2 sets (S2 and S3) were obtained for 24 h. The substrates were placed into polycarbonate Petri slide dishes, and were stored frozen until the analysis.

Atmospheric concentration of PM_{10} mass was also obtained from the closest measurement station of the National Air Quality Network in Budapest. This monitoring station is located in the upwind prevailing wind direction from the BpART facility in a distance of 1.6 km. It was measured by a continuous ambient particulate monitor (Thermo FH-62-IR), which is based on beta-ray attenuation, with a time resolution of 1 h. Total particle number concentrations ($N_{6–1000}$) and ultrafine (UF, d < 100 nm) particle number concentrations were derived from a differential mobility particle sizer (DMPS) system with a time resolution of 8 min (e.g. Salma et al., 2016). The DMPS measurements have been performed continuously and according to the recommendations of international technical standards. Local meteorological data including air temperature (T), RH and wind speed (WS) were obtained by standardised methods from a regular measurement station of the Hungarian Meteorological Service (HMS, no. 12843) situated near the BpART facility. Time resolution of these measurements was 10 min.

2.2. Chemical analyses

The PM mass concentrations on the impactor stages were obtained by gravimetric method, weighing each substrate before and after the sampling on a Sartorius MC 210P microbalance with a sensitivity of 5 μg. The filters were pre-equilibrated before weighing at a temperature of 19 ± 5 °C and RH between 40% and 50% for 24 h. Possible static electricity on the substrates were eliminated.

Half section of each impaction substrate was analysed for LVG, MAN and GAN by gas chromatography–mass spectrometry (GC–MS) after trimethylsilylation. The sections were extracted in glass beakers with 10 mL of absolute ethanol in an ultrasonic bath (Bandelin Sonorex, RK 52H) for 15 min. After decantation of the supernatant, the extraction step was repeated. The combined extracts were filtered through a PVDF syringe filter with a pore size of 0.22 μm and were spiked with an internal standard (IS) of methyl β-L-arabinopyranoside (1.54 ng μL^{-1}). Standards of LVG, MAN and GAN were dissolved in methanol (5–10 mg in 5 mL), were diluted 10–2000×, and finally, they were also spiked with 20–40 μL of IS. The sample extracts and standard solutions were evaporated to dryness with a rotary evaporator (Büchi Rotavapor R-200) at a temperature of 30–40 °C in 2–4 mL Reacti vials. The silylation chemical reaction was carried out by adding 200 μL hexamethyldisilazane (HMDS) as silylating agent, 125 μL pyridine as solvent and 25 μL trifluoroacetic acid as catalyst of the silylation to the evaporation residues at 70 °C for 90 min. All analytical reagents were of high purity grade, which means a purity of at least 99% except for MAN and GAN model compounds which had a purity of 95%. After the derivatisation, the aerosol samples were diluted 6× with HMDS, and the solutions were injected into a Varian 4000 GC–MS/MS system (Varian, USA) equipped with a Varian CP-8400 auto sampler and with a septum equipped CP-1079 programmable temperature vaporizer (PTV) injector. The GC column used was a SGE forte BPX-5 capillary (length × inner diameter 15 m × 0.25 mm; film thickness 0.25 μm, SGE, Australia). Helium (in a purity of 99.9999%) was utilised as carrier gas with a fixed column flow rate of 1 mL min^{-1}. The injection volumes were 1 μL in all cases with selecting the "on column" injection mode. The optimized temperature program for the PTV injector was the following: the injections were made at 100 °C, held for 0.5 min, then heated up to 280 °C with a rate of 200 °C min^{-1}, and finally held at this temperature for 3 min. The optimized temperature program for the column oven was the following: the column temperature program started at 100 °C, held for 1 min, heated up to 150 °C with a rate of 5 °C min^{-1}, then heated up to 300 °C with a rate of 20 °C min^{-1}, and finally held at this temperature for 2 min. The total program runtime was 21 min. The temperatures of the transfer line, ion trap and manifold were 280, 210 and 80 °C, respectively. The ionization voltage was 70 eV with an internal ionization option. The quantification was carried out in the selected ion monitoring mode by quantifier ions with mass-to-charge ratios of m/z = 204 for LVG and of 217 for MAN, GAN and IS standard. The retention times for GAN, MAN and LVG were 7.9, 8.1 and 8.4 min. Chromatograms containing the 4 derivatised compounds in a standard solution and for a real aerosol sample are shown in Fig. 1, which indicate that the selected peaks are well separated. The calibration curves consisting of 7 points covered the ranges of 0.05–10 ng μL^{-1} for LVG, 0.01–2.0 ng μL^{-1} for MAN and 0.005–1.0 ng μL^{-1} for GAN. The repeatability of the method was between 2% and 10% relative SD. The field blank samples were analysed utilising an analytical protocol that was identically to that for the aerosol samples, and each analytical series contained a blank sample. The limit of quantitation (LOQ) for LVG and MAN was approximately 0.7 ng m^{-3}, while it was approximately 0.3 ng m^{-3} for GAN.

Concentrations of K in the aerosol samples were determined by extracting the remaining half sections of the impactor substrate in 2.5 mL high-purity reagent Milli-Q water with an ultrasonic bath for 2 × 15 min. The water extracts were filtered through a PVDF syringe membrane filters with a pore size of 0.45 μm to remove the suspended insoluble particles, and 25 μL of ionization matrix which contained 100 mg mL^{-1} Cs and 50 mg mL^{-1} La was added to each sample. The measurements were accomplished by atomic absorption spectrometry with electrothermal atomization using an instrument AAnalyst 700 (Perkin Elmer, USA). The field blank samples were treated identically with the aerosol samples, and the analytical results were corrected for the blanks. The LOQ of the sampling and analytical procedure was approximately 0.2 ng m^{-3}; and the concentrations measured were several times above this limit.

The PM mass, LVG and K analytical data were corrected for blanks by subtracting the mean blank value from the corresponding amounts in real samples. The blank PM mass was determined from the full impaction foils; half section of each impaction substrate was utilised for determining the blank value for LVG, while the other half section was applied for deriving the blank values for K. The mean blanks and SDs were 25 ± 6 μg, 30 ± 8 and 81 ± 11 ng, respectively for the sample sections analysed. Mannosan and GAN were not detected in the blanks.

2.3. Data treatment

The concentration data sets obtained for LVG, MAN, GAN and K in the cascade impactor samples were inverted into size distributions by the computer program MICRON (Winklmayr et al., 1990; Wolfenbarger and Seinfeld, 1990). Its mathematical procedure is based on constrained regularisation. The data treatment takes into account both the concentration data on all impactor stages and the impaction efficiency curves for all stages. The SDs of the input concentration data, which are also needed for the inversion, were estimated by combining the relative SD for aerosol sampling and chemical analysis according to the propagation of errors in order to obtain more realistic overall SDs. The former uncertainty was estimated previously to be approximately 10% from a number of parallel samplings with two cascade impactors (Salma et al., 2004), while the latter uncertainty was determined by the analysis and ranged from 2% to 10%. With increasing input uncertainties, the peaks in the distributions become broader and somewhat smaller, while the modal concentrations and mass median aerodynamic diameters (MMADs) are ordinarily preserved. The increased uncertainties, however, disadvantageously affect the identification of modes with very small concentrations. As far as the impaction efficiency curves are concerned, they each contained at least 120 experimental data points of which, there were 30, 24, 15, 15, 15, 15, 24, 20, 34 and 34 relevant efficiency data between 10% and 90% for stages from 1 to 10, respectively. The inversion produced a smooth size distribution, which was represented by 80 inverted data points. The inverted data sets were then fitted by log-normal distributions so that the MMADs, geometric standard deviations (GSDs) and mass concentrations of the contributing modes are derived. The quality of the fit was usually good (reduced $\chi^2 \approx 1$), though in some particular cases and usually around the end points of the diameter interval investigated, the agreement between the inverted data and the fitted curve was less perfect. This is most likely caused by experimental fluctuations in the baseline concentrations, shifts of the modes during the sampling time periods (e.g. with changing RH) and/or by some possible sampling errors (e.g. due to bounce-off effect, Schwarz et al., 2012). To consider these artefacts as well, the relative uncertainty of a few particular concentrations at the diameter limits were increased up to 25%.

3. Results and discussion

Air T and RH varied over the sampling campaign between −2.4 and 11.8 °C and 58% and 92%, respectively. Their means and SDs derived for the separate sampling time intervals are summarised in Table 1 together with WS. The data indicate that the local weather during the collections of samples was mild and calm without extreme meteorological situations. It was also dry except for last sampling interval (S4) when there was a mixed precipitation of 7 mm composed of rain and

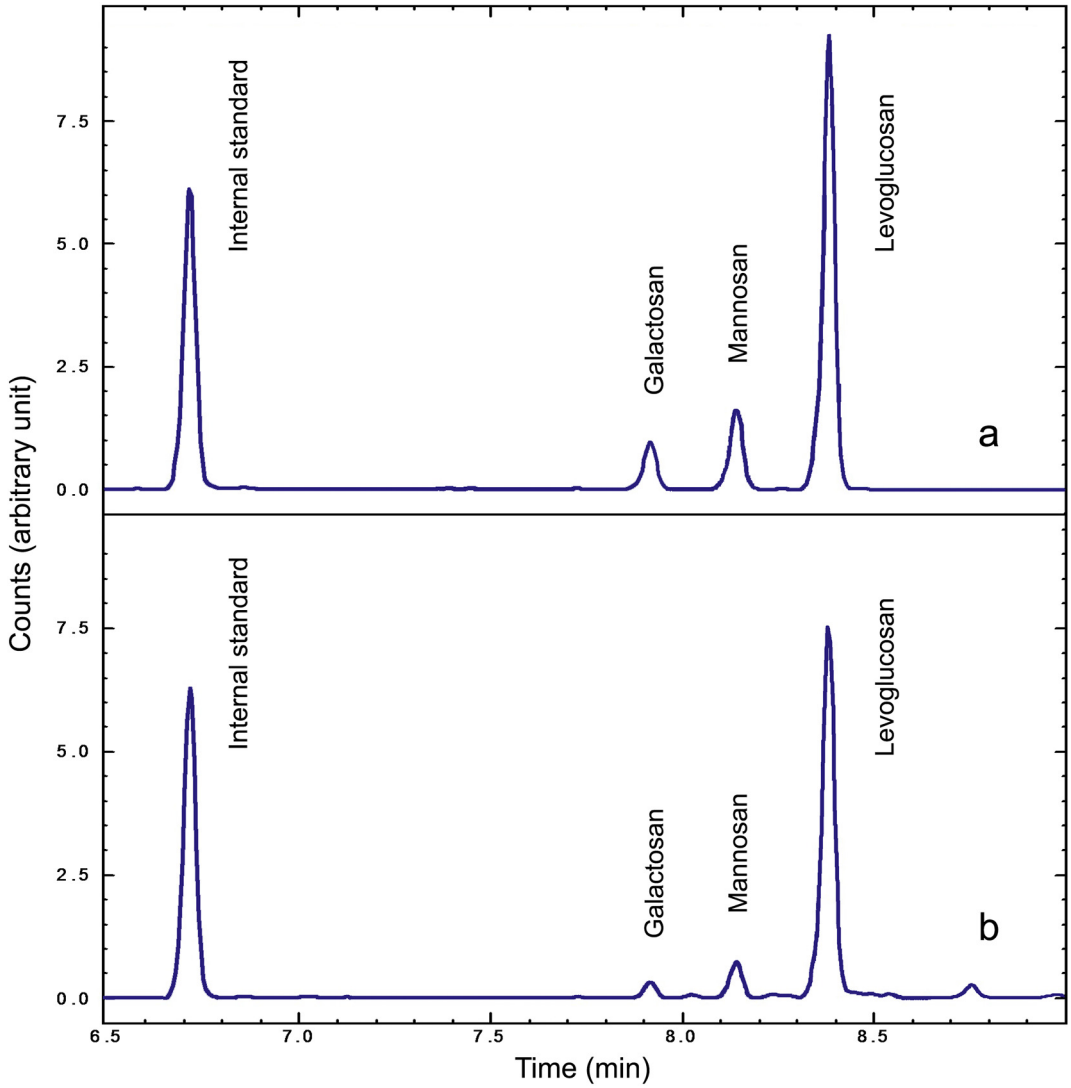

Fig. 1. GC–MS chromatograms of a standard solution containing 1.54 ng μL^{-1} methyl β-L-arabinopyranoside as internal standard, 0.20 ng μL^{-1} galactosan, 0.40 ng μL^{-1} mannosan and 2.0 ng μL^{-1} levoglucosan (a) and for the aerosol sample S4, impaction stage no. 6 (b) showing the separation of the trimethylsilyl ether derivatives of the compounds.

Table 1
Means and standard deviations (SDs) for air temperature (*T*), relative humidity (RH) and wind speed (WS) for separate sample collection time intervals S1-S4. The duration of the sampling intervals is also shown in brackets.

Property/Sampling interval	*T* (°C)		RH (%)		WS (m s^{-1})	
	Mean	SD	Mean	SD	Mean	SD
S1 (2 d)	6.7	2.7	76	9	2.5	1.8
S2 (1 d)	3.8	1.0	85	3	2.1	1.2
S3 (1 d)	7.5	2.4	75	9	1.9	1.1
S4 (2 d)	3.3	2.6	78	7	4.3	2.8

snow (on 28–12–2017). Strong wind up to 12.4 m s^{-1} occurred during this sampling interval (on 29–12–2017) as well.

3.1. Atmospheric concentrations

Atmospheric concentrations of total particle number, UF particles, particulate mass, K and monosaccharide anhydrides in various size fractions are shown in Table 2. Median total particle number concentrations were calculated from the individual DMPS data for the related consecutive sampling intervals. The particle number concentrations in Table 2 are in line with ordinary concentration levels in central Budapest. The annual median $N_{6–1000}$ in 2017 was 10.6×10^3 cm^{-3} with an annual mean UF concentration ratio and SD of (81 ± 10)%. Temporal variability in $N_{6–1000}$ and UF ratio in the consecutive sampling intervals can be explained by the effect of local meteorology on the air quality (Salma et al., 2014). The larger total concentrations and relatively low UF ratios for the sampling intervals S2 and S3 jointly suggest that during these days, the air masses which arrived to the receptor site brought in larger particle number concentrations from polluted regional areas, and that local (urban) high temperature sources were less intensive. These days seem, therefore, particularly important for studying the markers since BB is expected to mainly occur outside the city (Salma et al., 2017).

Concentrations in $PM_{9.9}$ and $PM_{3.1}$ were derived by summing up the concentrations for impactor stages with $d_{50} \leq 9.9$ μm and ≤ 3.1 μm, respectively. The former size fraction expresses the PM_{10} (which is often reported and used in health-related studies) well, while the latter (fine) size fraction represents a systematic overestimation of the $PM_{2.5}$ for chemical species which have a non-negligible relative concentration above the diameter of 2.5 μm. This is the case for the PM mass and K, while the concentrations of the monosaccharide anhydrides are

Table 2
Median total aerosol particle number concentrations ($N_{6\text{-}1000}$), ultrafine particle (UF) concentration ratios to the total particle numbers obtained from the DMPS system, and concentrations of particulate matter mass and K in the $PM_{9.9}$ size fraction, of levoglucosan (LVG), mannosan (MAN), galactosan (GAN) in the $PM_{3.1}$ size fractions as derived by summing up the concentrations for MOUDI stages with aerodynamic cut-off diameters of ≤ 9.9 μm and ≤ 3.1 μm, respectively. The $PM_{9.9}$ size fraction represents well the PM_{10}, while the $PM_{3.1}$ expresses well the $PM_{2.5}$ (fine) particles for the chemical species given. The sample labels are indicated together with the duration of the sampling intervals in brackets.

Size fraction/species/sample	$PM_{1.0}$		$PM_{9.9}$		$PM_{3.1}$		
	$N_{6\text{-}1000}$	UF ratio	Mass	K	LVG	MAN	GAN
	(10^3 cm^{-3})	(%)	(μg m^{-3})	(μg m^{-3})	(μg m^{-3})	(ng m^{-3})	(ng m^{-3})
S1 (2 d)	4.2	80	18.6	0.197	0.34	42	11.2
S2 (1 d)	11.3	61	43	0.52	0.85	98	35
S3 (1 d)	15.0	74	27	0.44	0.37	32	10.5
S4 (2 d)	6.6	80	11.2	0.150	0.177	17.8	5.8

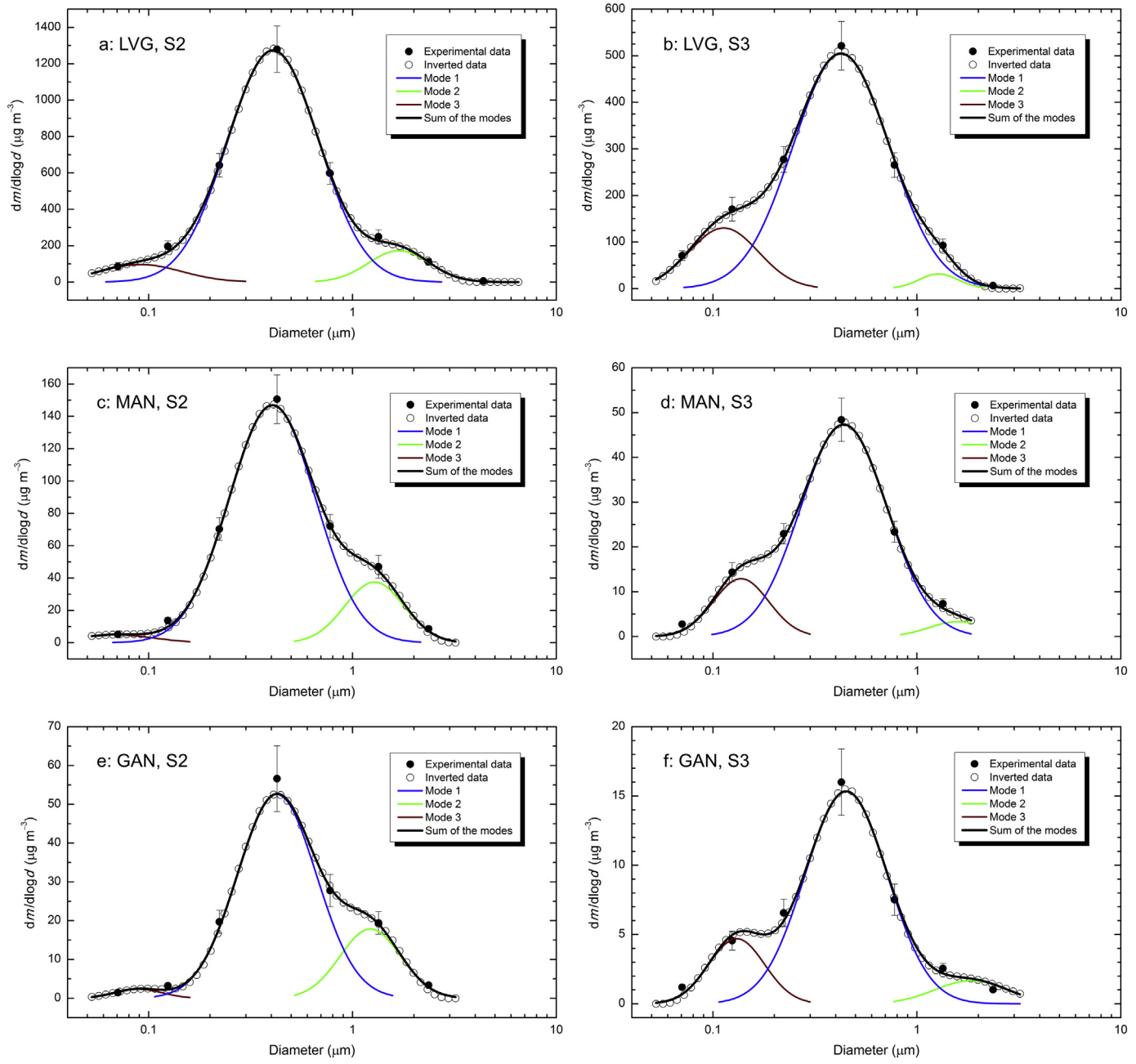

Fig. 2. Modal structure of mass size distributions of levoglucosan (LVG, a and b), mannosan (MAN, c and b) and galactosan (GAN, e and f) in the most loaded samples (S2 and S3). The modes 1, 2 and 3 were assigned to the condensation submode and droplet submode of the major accumulation mode and to a minor accumulation mode, respectively. The error bars indicate ± 1 overall standard deviations.

representative for $PM_{2.5}$ as well (see Section 3.2.). The cut-off value at 3.1 μm was also selected by considering that the contribution of monosaccharide anhydrides in the diameter interval between 2.5 and 3.1 μm to their total amount is negligible, while their contribution in the interval 1.8–2.5 μm is larger (see Fig. 2.). Median $PM_{9.9}$ and $PM_{3.1}$ mass concentrations for the all samples were 23 and 20 μg m^{-3}, which indicate relatively clean atmospheric situations in the city. The medians are below the EU daily mean PM_{10} health limit and annual mean $PM_{2.5}$ target value, respectively. It is noted that the concentrations were obtained during Christmas time and festive season, when the urban vehicular road traffic is usually lower and the house heating and cooking activities including BB are expected to be larger. Daily ranges and medians of the PM_{10} mass concentration obtained from the air quality monitoring network for the sampling campaign were 3–19 and 8.5, 6–59 and 16.0, 30–55 and 46, 23–66 and 42, 8–37 and 19.0 and 3–21 and 10.5 μg m^{-3}, respectively. The concentration level was low in the first and the last 2 days, which was the main reason for selecting the consecutive sampling time intervals for 2, 1, 1 and 2 d, respectively. The $PM_{9.9}$ mass from the MOUDI was compared to the mean PM_{10} mass derived by averaging the individual on-line concentrations from the monitoring station for the time intervals that correspond to the sample collection intervals. A mean MOUDI/monitor concentration ratio and SD of 84 ± 11% were obtained. This is a reasonable agreement, which indicates that the overall operation of the impactor is acceptable. Median atmospheric concentration of K in the $PM_{9.9}$ size fraction was 0.32 μg m^{-3}. This agrees well with the mean of 0.36 μg m^{-3} at STP reported earlier for PM_{10} filter based aerosol samples collected in the city centre in springtime (Salma et al., 2002).

Median atmospheric concentrations of LVG, MAN and GAN for all samples were 0.36 μg m^{-3}, 37 and 10.9 ng m^{-3}, respectively. These data are comparable to median concentrations of 0.40 μg m^{-3}, 25 and 16.1 ng m^{-3}, respectively which were obtained for the $PM_{2.5}$ size fraction at the same site in winter 2014 (Salma et al., 2017). The concentrations of monosaccharide anhydrides are also comparable to those in other urban sites in Europe in winter (e.g. Szidat et al., 2009; Maenhaut et al., 2012, 2016; Schwarz et al., 2016). Their ordinary concentrations exhibit a pronounced seasonal variation with a maximum in winter (Caseiro et al., 2009; Kourtchev et al., 2011; Maenhaut et al., 2012, 2016; Wang et al., 2018), which suggests that residential wood burning preferably occurs in the colder months.

3.2. Size distributions

The mass size distributions of markers consisted of several modes. The distributions of the monosaccharide anhydrides were fitted by 3 separate modes in order to avoid systematic differences in the residuals. Their distributions are shown in Fig. 2 for the 2 most loaded samples as examples, and their mean modal parameters are summarised in Table 3. All distributions contained a dominant accumulation mode (labelled as mode 1) with a typical MMAD of 0.42 μm. Its relative modal concentration (RMC) varied between 85% and 90% for all monosaccharide anhydrides. It is undoubtedly caused by BB. The accumulation mode is sometimes split into condensation and droplet submodes (Hering and Friedlander, 1982; John et al., 1999, Hering et al., 1997). The splitting is produced by water activation of condensation submode particles under high RH conditions to form cloud droplets, followed by dissolution of some atmospheric gases (e.g. SO_2 or some polar VOCs, which can be present in relatively large concentrations inside smoke plumes) into the droplets, and finally, by aqueous-phase chemical oxidation reactions leading to less volatile products. If the ambient RH decreases at a later time and the droplets evaporate, the remaining solid particles have larger diameters than the original dry particles (Meng and Seinfeld, 1994; Kerminen and Wexler, 1995; Salma et al., 2005). This splitting of the dominant accumulation mode was also observed for all monosaccharide anhydrides. In some cases such as in Fig. 2a, c and e for LVG, MAN and GAN, respectively, the droplet submode (mode 2 in Fig. 2 and Table 3) was obviously present, and showed a typical MMAD from 1.4 to 1.7 μm. In some other cases such as in Fig. 2b, d and f, the droplet submode may be not significant. It could be so small or even missing that the related peak was just generated by the inversion procedure from the fluctuating concentration data as an artefact. It is worth mentioning for the comparison that the droplet submodes for water-soluble organic carbon (WSOC) and atmospheric humic-like substances (HULIS) were obviously identified earlier at the same location (Salma et al., 2013). Its MMADs of 1.72 μm for WSOC and 1.22 μm for HULIS are similar to those for the monosaccharide anhydrides. The size distributions of WSOC and HULIS also contained an evident coarse mode with a typical MMAD of 6.4 μm. These 2 conclusions confirm the assignment of the mode 2 to the droplet submode (and not to a coarse mode), and it is also strengthened by the size distributions of K (see below). The absence of the coarse modes of LVG, MAN and GAN implies that their resuspension processes are negligible relative to their burning-related sources. This could be different for field fires. Mode 3 in the size distributions showed typical MMADs at 0.11 μm and RMCs of up to 9%. Similarly to the droplet submode, its presence was obvious in some cases (Fig. 2b, d and f), while it may be not significant in some other cases (Fig. 2a, c and e). The mode 3 is expected to be generated by another source which is realised at higher burning temperatures than BB since it has smaller MMADs than the mode 1. Fossil fuel combustion was reported to produce smaller aerosol particles than BB (Yang et al., 2006), which implies that the additional emission source could be lignite combustion. The final association can be validated by dedicated measurements. Nevertheless, the mean contribution of lignite to the LVG seems small (5%) or negligible when compared to its experimental uncertainty. This could justify that the lignite combustion is usually neglected as an LVG source in BB studies. The dominant accumulation modes of LVG, MAN and GAN were found to be quite uniform and consistent, which can be associated with the abundance and intensity of their major sources in the area on a time scale of their atmospheric lifetime of approximately 10 d. Contributions of the other 2, much smaller modes varied considerably, which suggests that their major sources and atmospheric transformation processes change with environmental conditions or air mass trajectories (more localised source).

There are only a few studies which dealt with the size distribution of LVG. They reported unimodal size distributions with MMADs between 0.7 and 1.1 μm (Wang et al., 2009) and of 0.5 μm (Gaughan et al., 2014). All these distributions were generated without inverting the experimental concentrations, and were plotted as column graphs. This representation, however, does not make it feasible to derive detailed size distributions and characteristics. The former interval was obtained under haze conditions caused by wheat straw burning and non-haze conditions in Nanjing, China by using an Andersen cascade impactor. The difference in the MMADs for our major accumulation mode (at 0.42 μm) and the fine mode in that study could be related to the wheat straw burning, which occurs at lower temperatures than wood burning (as it was in our case, see Section 3.3.), and, which, therefore, tends to

Table 3
Mean values of mass median aerodynamic diameters (MMAD) in a unit of μm, geometric standard deviations (GSD) and relative modal concentrations (RMC) in a unit of % for separate modes in the mass size distributions of levoglucosan, mannosan and galactosan. The modes 1, 2 and 3 were assigned to the condensation submode and droplet submode of the major accumulation mode and to a minor accumulation mode, respectively.

Species/	Levoglucosan			Mannosan			Galactosan		
Property/ mode	MMAD	GSD	RMC	MMAD	GSD	RMC	MMAD	GSD	RMC
Mode 1	0.41	1.71	90	0.42	1.65	89	0.43	1.61	85
Mode 2	1.70	1.39	5	1.43	1.38	9	1.74	1.52	12
Mode 3	0.11	1.54	9	0.12	1.50	9	0.10	1.40	8

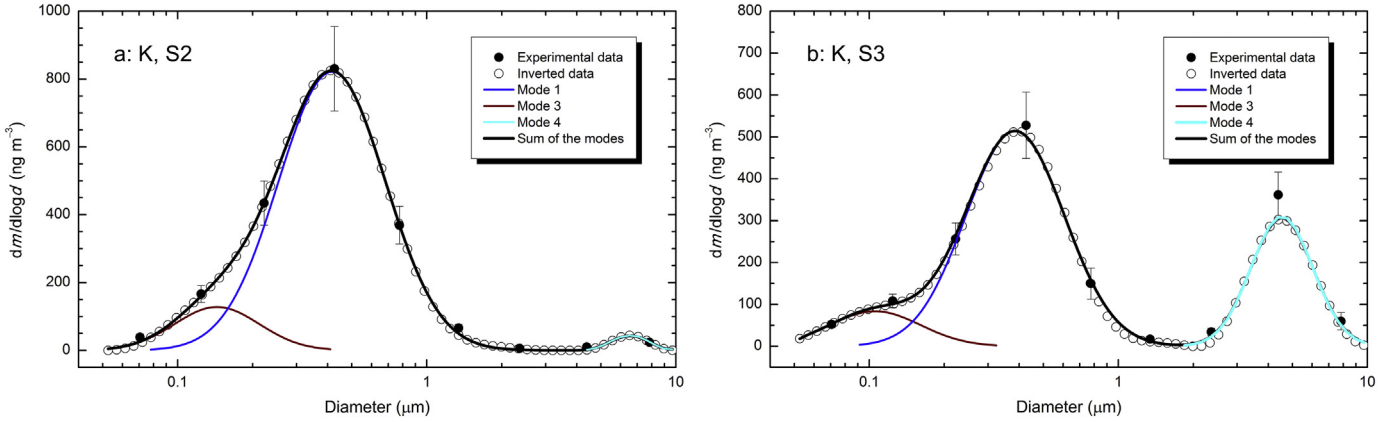

Fig. 3. Modal structure of mass size distributions of K in the most loaded samples (S2 and S3). Modes 1, 3 and 4 were assigned to a major accumulation mode, minor accumulation mode and coarse mode, respectively. The error bars indicate ± 1 overall standard deviations.

generate relatively larger particles (Yang et al., 2006). Another explanation could be that the MOUDI sampler has 6, well spread impaction stages in the submicrometer diameter range down to 0.053 μm (see Section 2.1.), while the Andersen cascade impactor (most commonly used for testing inhaled pharmaceutical products) has only 3 stages (with d_{50}s of 1.1, 0.7 and 0.4 μm) in the corresponding diameter range. The MMAD in the latter publication was obtained by using personal cascade impactors attached on wildland firefighters, and agrees well with our corresponding value.

For K, 3 modes were also identified in the size distributions. (They were numbered as 1, 3 and 4 to maintain the consistency with the monosaccharide anhydrides.) Some size distributions are shown in Fig. 3 as examples. The mean MMADs, GSDs and RMCs of the 3 contributing modes were 0.40 μm, 1.66 and 78% for the mode 1, 0.16 μm, 1.61 and 16% for the mode 3, and 5.8 μm, 1.45 and 10% for the mode 4. The modes 1 and 2 were assigned to the major and minor accumulation modes similarly to the monosaccharide anhydrides, while the mode 4 is an evident coarse mode. Major emission sources of coarse K could be the disintegration and suspension processes of crustal rock and soil. Potassium was determined after a water extraction, and, therefore, its concentration only represents the water-soluble chemical forms, primarily K^+ cation. Particles generated from continental surfaces are expected to mainly contain K in water insoluble molecules (such as alkali feldspars), which would make the coarse mode of the total K larger or very substantial in accordance with earlier local studies (e.g. Salma et al., 2002, 2005). The overall size distributions of fine K are also consistent with earlier results (e.g. Schwarz et al., 2012), and follow the distributions of the monosaccharide anhydrides.

3.3. Relationships and contributions

Considerable linear relationships among the monosaccharide anhydrides were observe although the number of samples is rather limited. Fortunately, the ranges of the concentrations were relatively large. The Pearson's coefficients of correlation between LVG on one side and MAN, GAN and fine K on the other side were 0.99, 0.99 and 0.86, respectively, while MAN correlated with GAN with a coefficient of 0.99. The relationships are significant at a joint $p = .1$ level, and are in line with earlier results (e.g. Zhang et al., 2014). This suggests that their major source is common, which is undoubtedly residential BB. Coefficients of correlation between PM_{10} mass on one side and the monosaccharide anhydrides on the other side were smaller, typically between 0.91 and 0.96. Conclusive interpretation of these correlations is restricted by the limited number of samples. Levoglucosan was utilised to estimate the amount of the PM originating from BB. Several PM_{10} mass/LVG conversion factors have been used in the literature; they were reviewed by Puxbaum et al. (2007). The conversion factor depends on the burning conditions and biofuel types. We adopted a factor of 10.7, which was suggested by Schmidl et al. (2008) for the mix of wood used in Austria. Based on our previous local experience (e.g. Salma et al., 2017) and international practice (e.g. Szidat et al., 2009; Maenhaut et al., 2012, 2016), this seems to be a reasonable approximation to reality for our conditions as well. The uncertainty of the conversion was estimated to be approximately 30% (Maenhaut et al., 2012). Contribution of BB to the PM_{10} mass estimated in this way ranged from 15% to 21% with a mean and SD of 18 ± 3%. This is in good agreement with a mean contribution and SD of 11 ± 3% determined from aerosol filter samples at the same site for the mild winter of 2014 (Salma et al., 2017). Biomass burning represents a considerable or substantial source for PM_{10} mass in the Budapest area. The present results and conclusions are also in line with winter data from various other locations in European cities (Pashynska et al., 2002; Szidat et al., 2009; Piazzalunga et al., 2011; Caseiro and Oliveira, 2012; Maenhaut et al., 2012, 2016; Schwarz et al., 2016).

Concentration ratio LVG/(MAN+GAN) was proposed to differentiate between wood burning and other BB emissions, while the ratio LVG/MAN was applied to distinguish between hardwood and softwood burning (Fine et al., 2004; Schmidl et al., 2008; Fabbri et al., 2009; Caseiro et al., 2009; Favez et al., 2010; Piazzalunga et al., 2011; Maenhaut et al., 2012). The typical ranges of the two ratios for different BB fuel types were overviewed by Maenhaut et al. (2012). Combustion of Miocene lignite exhibits an identical LVG/(MAN + GAN) and LVG/MAN ratios of approximately 54. Softwood combustion typically yields LVG/(MAN + GAN) and LVG/MAN ratios smaller than 3 and 4, respectively, while the same ratios for hardwood emissions are 8.5–9.9 and 14–15, respectively. Derivatives of crude oil, natural gas, coal and biomass are the major carbonaceous fuel types utilised in Hungary; peat is not burned. The major form of solid fuels is lignite/brown coal, which makes up approximately 88% of the consumption when expressed in tons utilised. For our samples, the LVG/(MAN + GAN) ratios ranged from 6.3 to 8.8 with a mean and SD of 7.3 ± 1.2, while the LVG/MAN ratio varied from 8.1 to 11.7 with a mean and SD of 9.6 ± 1.6. The means are close to the values characterising wood combustion, particularly hardwood emissions. The ratios also can indicate indirectly that lignite combustion a small or even a negligible contribution to the monosaccharide anhydrides. This is in line with the conclusion obtained from the LVG, MAN and GAN size distributions.

The mean LVG/MAN ratio was further utilised to roughly estimate the share of softwood (ordinary spruce) burnt relative to the hardwood burnt according to the empirical relationship of %spruce = (14.8–LVG/MAN)/0.112 (Schmidl et al., 2008). This dependency was originally set for the combustion of common hardwood (beech and oak) and softwood species (spruce and larch) in typical wood stoves in Austria. For our samples, all individual LVG/MAN ratios were smaller than 14.8.

The percentage of spruce burned relative to the hardwood in the Budapest area was estimated in this way to be 46%.

4. Conclusions

Importance of BB for air quality considerations is increasingly recognised. One of the most straightforward methods of estimating the share of BB on PM mass or OC is based on LVG as a single marker. Its possible emissions from lignite combustion are ordinarily neglected. This can be backed by carbonaceous fuel inventory for a region or country. Here we present a complementary method based on detailed mass size distributions, which can be applied to estimate the contribution of lignite combustion to LVG concentrations. In the Budapest area, its relative contribution was approximately 5%, which is within usual experimental uncertainty of atmospheric concentrations, and, therefore, it can indeed be neglected. A limitation of this study lays in the restricted number of samples. A dedicated source apportionment survey involving BB at the city centre, suburb and regional background of Budapest based on aerosol samples collected on filters for 1 full year has been in progress, and its perspective results and conclusions are to add on the seasonal variability of the BB emissions and are to increase the representativity and reliability of the present conclusions as well.

It was pointed out in a recent study (Maenhaut et al., 2016) that the PM_{10}/LVG conversion factor of Schmidl et al. (2008) may be substantially underestimated for other conditions and sites than originally considered, which implies that the real importance of wood burning in many areas could be much larger than previously thought. Studies that apply both the LVG marker method and e.g. statistical approaches are desired for more accurate estimations.

The most severe daily PM_{10} health limit exceedances in many cities occur in winter, when the contribution of BB is expected to be the largest. This offers a considerable potential for improving the air quality by improvements in technological specifications for various household appliances that burn biomass together with efficient training of their users.

Acknowledgements

Financial support by the National Research, Development and Innovation Office, Hungary (contract K116788) and by the European Regional Development Fund and the Hungarian Government (GINOP-2.3.2-15-2016-00028) is gratefully acknowledged. The authors thank J. D. Varga of the Eötvös University for her help in the sample preparation for the GC–MS analysis and A. Machon of the Hungarian Meteorological Service for his help in the AAS analysis.

References

Bernardoni, V., Calzolai, G., Chiari, M., Fedi, M., Lucarelli, F., Nava, S., Piazzalunga, A., Riccobono, F., Taccetti, F., Valli, G., Vecchi, R., 2013. Radiocarbon analysis on organic and elemental carbon in aerosol samples and source apportionment at an urban site in Northern Italy. J. Aerosol Sci. 56, 88–99.

Caseiro, A., Oliveira, C., 2012. Variations in wood burning organic marker concentrations in the atmospheres of four European cities. J. Environ. Monit. 14, 2261–2269.

Caseiro, A., Bauer, H., Schmidl, C., Pio, C.A., Puxbaum, H., 2009. Wood burning impact on PM10 in three Austrian regions. Atmos. Environ. 43, 2186–2195.

Chen, J., Li, Ch., Ristovski, Z., Milic, A., Gu, Y., Islam, M.S., Wang, S., Hao, J., Zhang, H., He, C., Guo, H., Fu, H., Miljevic, B., Morawska, L., Thai, P., Lam, Y.F., Pereira, G., Ding, A., Huang, X., Dumka, U.C., 2017. A review of biomass burning: emissions and impacts on air quality, health and climate in China. Sci. Total Environ. 579, 1000–1034.

Claeys, M., Kourtchev, I., Pashynska, V., Vas, G., Vermeylen, R., Wang, W., Cafmeyer, J., Chi, X., Artaxo, P., Andreae, M.O., Maenhaut, W., 2010. Polar organic marker compounds in atmospheric aerosols during the LBA-SMOCC 2002 biomass burning experiment in Rondônia, Brazil: sources and source processes, time series, diel variations and size distributions. Atmos. Chem. Phys. 10, 9319–9331.

Claeys, M., Vermeylen, R., Yasmeen, F., Gómez-González, Y., Chi, X., Maenhaut, W., Mészáros, T., Salma, I., 2012. Chemical characterisation of humic-like substances from urban, rural and tropical biomass burning environments using liquid chromatography with UV/vis photodiode array detection and electrospray ionisation mass spectrometry. Environ. Chem. 9, 273–284.

Fabbri, D., Marynowski, L., Fabiańska, M.J., Zaton, M., Simoneit, B.R.T., 2008. Levoglucosan and other cellulose markers in pyrolysates of miocene lignites: Geochemical and environmental implications. Environ. Sci. Technol. 42, 2957–2963.

Fabbri, D., Torri, C., Simoneit, B.R.T., Marynowski, L., Rushdi, A.I., Fabiańska, M.J., 2009. Levoglucosan and other cellulose and lignin markers in emissions from burning of Miocene lignites. Atmos. Environ. 43, 2286–2295.

Favez, O., El Haddad, I., Piot, C., Boréave, A., Abidi, E., Marchand, N., Jaffrezo, J.-L., Besombes, J.-L., Personnaz, M.-B., Sciare, J., Wortham, H., George, C., D'Anna, B., 2010. Inter-comparison of source apportionment models for the estimation of wood burning aerosols during wintertime in an Alpine city (Grenoble, France). Atmos. Chem. Phys. 10, 5295–5314.

Fine, P.M., Cass, G.R., Simoneit, B.R.T., 2004. Chemical characterization of fine particle emissions from the fireplace combustion of wood types grown in the Midwestern and Western United States. Environ. Eng. Sci. 21, 387–409.

Fraser, M.P., Lakshmanan, K., 2000. Using levoglucosan as a molecular marker for the long range transport of biomass combustion aerosols. Environ. Sci. Technol. 34, 4560–4564.

Gaughan, D.M., Piacitelli, Ch.A., Chen, B.T., Law, B.F., Virji, M.A., Edwards, N.T., Enright, P.L., Schwegler-Berry, D.E., Leonard, S.S., Wagner, G.R., Kobzik, L., Kales, S.N., Hughes, M.D., Christiani, D.C., Siegel, P.D., Cox-Ganser, J.M., Hoover, M.D., 2014. Exposures and cross-shift lung function declines in wildland firefighters. J. Occup. Environ. Hyg. 11, 591–603.

Gilardoni, S., Vignati, E., Cavalli, F., Putaud, J.P., Larsen, B.R., Karl, M., Stenström, K., Genberg, J., Henne, S., Dentener, F., 2011. Better constraints on sources of carbonaceous aerosols using a combined 14C – macro tracer analysis in a European rural background site. Atmos. Chem. Phys. 11, 5685–5700.

Hays, M.D., Smith, N.D., Kinsey, J., Dong, Y., Kariher, P., 2003. Polycyclic aromatic hydrocarbon size distributions in aerosols from appliances of residential wood combustion as determined by direct thermal desorption-GC/MS. J. Aerosol Sci. 34, 1061–1084.

Hennigan, C.J., Sullivan, A.P., Collett Jr., J.L., Robinson, A.L., 2010. Levoglucosan stability in biomass burning particles exposed to hydroxyl radicals. Geophys. Res. Lett. 37, L09806. https://doi.org/10.1029/2010GL043088.

Herich, H., Gianini, M.F.D., Piot, C., Močnik, G., Jaffrezo, J.L., Besombes, J.L., Prévôt, A.S.H., Hueglin, C., 2014. Overview of the impact of wood burning emissions on carbonaceous aerosols and PM in large parts of the Alpine region. Atmos. Environ. 89, 64–75.

Hering, S.V., Friedlander, S.K., 1982. Origins of aerosol sulfur size distribution in the Los Angeles Basin. Atmos. Environ. 16, 2647–2656.

Hering, S., Eldering, A., Seinfeld, J.H., 1997. Bimodal character of accumulation mode aerosol mass distributions in Southern California. Atmos. Environ. 31, 1–11.

Hoffmann, D., Tilgner, A., Iinuma, Y., Herrmann, H., 2010. Atmospheric stability of levoglucosan: a detailed laboratory and modelling study. Environ. Sci. Technol. 44, 694–699.

Hopke, Ph.K., 2016. Review of receptor modeling methods for source apportionment. J. Air Waste Manage. Assoc. 66, 237–259.

Iinuma, Y., Bruggemann, E., Gnauk, T., Muller, K., Andreae, M.O., Helas, G., Parmar, R., Herrmann, H., 2007. Source characterization of biomass burning particles: the combustion of selected European conifers, African hardwood, savanna grass, and German and Indonesian peat. J. Geophys. Res. 112, D08209. https://doi.org/10.1029/2006JD007120.

John, W., Wall, S.M., Ondo, J.L., Winklmayr, W., 1999. Modes in the size distributions of atmospheric inorganic aerosol. Atmos. Environ. 24A, 2349–2350.

Kerminen, V.-M., Wexler, A.S., 1995. Growth laws of atmospheric aerosol particles: an examination of the bimodality of the accumulation mode. Atmos. Environ. 22, 3263–3275.

Kourtchev, I., Hellebust, S., Bell, J.M., O'Connor, I.P., Healy, R.M., Allanic, A., Healy, D., Wenger, J.C., Sodeau, J.R., 2011. The use of polar organic compounds to estimate the contribution of domestic solid fuel combustion and biogenic sources to ambient levels of organic carbon and PM2.5 in Cork Harbour, Ireland. Sci. Total Environ. 409, 2143–2155.

del Águila, A., Sorribas, M., Lyamani, H., Titos, G., Olmo, F., Arruda-Moreira, G., Yela, M., Alados-Arboledas, L., 2018. Sources and physicochemical characteristics of submicron aerosols during three intensive campaigns in Granada (Spain). Atmos. Res. 213, 398–410.

Locker, H.B., 1988. The Use of Levoglucosan to Assess the Environmental Impact of Residential Wood Burning on Air Quality (Ph. D. Thesis). Dartmouth College, Hanover.

Maenhaut, W., Salma, I., Cafmeyer, J., Annegarn, H.J., Andreae, M.O., 1996. Regional atmospheric aerosol composition and sources in the Eastern Transvaal, South Africa, and impact of biomass burning. J. Geophys. Res. 101, 23631–23650.

Maenhaut, W., Vermeylen, R., Claeys, M., Vercauteren, J., Matheeussen, C., Roekens, E., 2012. Assessment of the contribution from wood burning to the PM_{10} aerosol in Flanders, Belgium. Sci. Total Environ. 437, 226–236.

Maenhaut, W., Vermeylen, R., Claeys, M., Vercauteren, J., Roekens, E., 2016. Sources of the PM_{10} aerosol in Flanders, Belgium, and re-assessment of the contribution from wood burning. Sci. Total Environ. 562, 550–560.

Marple, V.A., Rubow, K.L., Behm, S.M., 1991. A Microorifice Uniform Deposit Impactor (MOUDI): description, calibration, and use. Aerosol Sci. Technol. 14, 434–446.

Meng, Z., Seinfeld, J.H., 1994. On the source of the submicrometer droplet mode of urban and regional aerosols. Aerosol Sci. Technol. 20, 253–265.

Minguillón, M.C., Perron, N., Querol, X., Szidat, S., Fahrni, S.M., Alastuey, A., Jimenez, J.L., Mohr, C., Ortega, A.M., Day, D.A., Lanz, V.A., Wacker, L., Reche, C., Cusack, M., Amato, F., Kiss, G., Hoffer, A., Decesari, S., Moretti, F., Hillamo, R., Teinilä, K., Seco, R., Peñuelas, J., Metzger, A., Schallhart, S., Müller, M., Hansel, A., Burkhart, J.F., Baltensperger, U., Prévôt, A.S.H., 2011. Fossil versus contemporary sources of fine

elemental and organic carbonaceous particulate matter during the DAURE campaign in Northeast Spain. Atmos. Chem. Phys. 11, 12067–12084.
Nolte, C.G., Schauer, J.J., Cass, G.R., Simoneit, B.R.T., 2001. Highly polar organic compounds present in wood smoke and in the ambient atmosphere. Environ. Sci. Technol. 35, 1912–1919.
Pashynska, V., Vermeylen, R., Vas, G., Maenhaut, W., Claeys, M., 2002. Development of a gas chromatography/ion trap mass spectrometry method for the determination of levoglucosan and saccharidic compounds in atmospheric aerosols, application to urban aerosols. J. Mass Spectrom. 37 1249–125.
Piazzalunga, A., Belis, C., Bernardoni, V., Cazzuli, O., Fermo, P., Valli, G., Vecchi, R., 2011. Estimates of wood burning contribution to PM by the macro-tracer method using tailored emission factors. Atmos. Environ. 45, 6642–6649.
Puxbaum, H., Caseiro, A., Sanchez-Ochoa, A., Kasper-Giebl, A., Claeys, M., Gelencsér, A., Legrand, M., Preunkert, S., Pio, C., 2007. Levoglucosan levels at background sites in Europe for assessing the impact of biomass combustion on the European aerosol background. J. Geophys. Res. 112, D23S05. https://doi.org/10.1029/2006JD008114.
Saarikoski, S., Sillanpaa, M., Sofiev, M., Timonen, H., Saarnio, K., Teinela, K., Karppinen, A., Kukkonen, J., Hillamo, R., 2007. Chemical composition of aerosols during a major biomass burning episode over northern Europe in spring 2006: experimental and modelling assessments. Atmos. Environ. 41, 3577–3589.
Saarikoski, S., Timonen, H., Saarnio, K., Aurela, M., Järvi, L., Keronen, P., Kerminen, V.-M., Hillamo, R., 2008. Sources of organic carbon in fine particulate matter in northern European urban air. Atmos. Chem. Phys. 8, 6281–6295.
Saarnio, K., Niemi, J.V., Saarikoski, S., Aurela, M., Timonen, H., Teinilä, K., Myllynen, M., Frey, A., Lamberg, H., Jokiniemi, J., Hillamo, R., 2012. Using monosaccharide anhydrides to estimate the impact of wood combustion on fine particles in the Helsinki Metropolitan Area. Boreal Environ. Res. 17, 163–183.
Salma, I., Maenhaut, W., Záray, Gy, 2002. Comparative study of elemental mass size distributions in urban atmospheric aerosol. J. Aerosol Sci. 33, 339–356.
Salma, I., Chi, X., Maenhaut, W., 2004. Elemental and organic carbon in urban canyon and background environments in Budapest, Hungary. Atmos. Environ. 38, 27–36.
Salma, I., Ocskay, R., Raes, N., Maenhaut, W., 2005. Fine structure of mass size distributions in urban environment. Atmos. Environ. 39, 5363–5374.
Salma, I., Ocskay, R., Chi, X., Maenhaut, W., 2007. Sampling artefacts, concentrations and chemical composition of fine water-soluble organic carbon and humic-like substances in a continental urban atmospheric environment. Atmos. Environ. 41, 4106–4118.
Salma, I., Mészáros, T., Maenhaut, W., 2013. Mass size distribution of carbon in atmospheric humic-like substances and water soluble organic carbon for an urban environment. J. Aerosol Sci. 56, 53–60.
Salma, I., Borsós, T., Németh, Z., Weidinger, T., Aalto, T., Kulmala, M., 2014. Comparative study of ultrafine atmospheric aerosol within a city. Atmos. Environ. 92, 154–161.
Salma, I., Németh, Z., Weidinger, T., Kovács, B., Kristóf, G., 2016. Measurement, growth types and shrinkage of newly formed aerosol particles at an urban research platform. Atmos. Chem. Phys. 16, 7837–7851.
Salma, I., Németh, Z., Weidinger, T., Maenhaut, W., Claeys, M., Molnár, M., Major, I., Ajtai, T., Utry, N., Bozóki, Z., 2017. Source apportionment of carbonaceous chemical species to fossil fuel combustion, biomass burning and biogenic emissions by a coupled radiocarbon–levoglucosan marker method. Atmos. Chem. Phys. 17, 13767–13781.
Sandradewi, J., Prévôt, A.S.H., Szidat, S., Perron, N., Rami Alfarra, M., Lanz, V.A., Weingartner, E., Baltensperger, U., 2008a. Using aerosol light absorption measurements for the quantitative determination of wood burning and traffic emission contributions to particulate matter. Environ. Sci. Technol. 42, 3316–3323.
Sandradewi, J., Prévôt, A.S.H., Weingartner, E., Schmidhauser, R., Gysel, M., Baltensperger, U., 2008b. A study of wood burning and traffic aerosols in an Alpine valley using a multi-wavelength Aethalometer. Atmos. Environ. 42, 101–112.
Schmidl, C., Marr, L.L., Caseiro, A., Kotianova, P., Berner, A., Bauer, H., Kasper-Giebl, A., Puxbaum, H., 2008. Chemical characterisation of fine particle emissions from wood stove combustion of common woods growing in mid-European Alpine regions. Atmos. Environ. 42, 126–141.
Schwarz, J., Štefancová, L., Maenhaut, W., Smolík, J., Ždímal, V., 2012. Mass and chemically speciated size distribution of Prague aerosol using an aerosol dryer - the influence of air mass origin. Sci. Total Environ. 437, 348–362.
Schwarz, J., Cusack, M., Karban, J., Chalupníčková, E., Havránek, V., Smolík, J., Ždímal, V., 2016. $PM_{2.5}$ chemical composition at a rural background site in Central Europe, including correlation and air mass back trajectory analysis. Atmos. Res. 176–177, 108–120.
Simoneit, B.R.T., Schauer, J.J., Nolte, C.G., Oros, D.R., Elias, V.O., Fraser, M.P., Rogge, W.F., Cass, G.R., 1999. Levoglucosan, a tracer for cellulose in biomass burning and atmospheric particles. Atmos. Environ. 33, 173–182.
Simoneit, B.R.T., Elias, V.O., Kobayashi, M., Kawamura, K., Rushdi, A.I., Medeiros, P.M., Rogge, W.F., Didyk, B.M., 2004. Sugars-dominant water-soluble organic compounds in soils and characterization as tracers in atmospheric particulate matter. Environ. Sci. Technol. 38, 5939–5949.
Szidat, S., Jenk, T.M., Synal, H.A., Kalberer, M., Wacker, L., Hajdas, I., Kasper-Giebl, A., Baltensperger, U., 2006. Contributions of fossil fuel, biomass-burning, and biogenic emissions to carbonaceous aerosols in Zurich as traced by ^{14}C. J. Geophys. Res. 111, D07206. https://doi.org/10.1029/2005JD006590.
Szidat, S., Ruff, M., Perron, N., Wacker, L., Synal, H.-A., Hallquist, M., Shannigrahi, A.S., Yttri, K.E., Dye, C., Simpson, D., 2009. Fossil and non-fossil sources of organic carbon (OC) and elemental carbon (EC) in Göteborg, Sweden. Atmos. Chem. Phys. 9, 1521–1535.
Vicente, E.D., Alves, C.A., 2018. An overview of particulate emissions from residential biomass combustion. Atmos. Res. 199, 159–185.
Wang, G., Kawamura, K., Xie, M., Hu, S., Cao, J., An, Z., Watson, J.G., Chow, J.C., 2009. Organic molecular compositions and size distributions of Chinese summer and autumn aerosols from Nanjing: characteristic haze event caused by wheat straw burning. Environ. Sci. Technol. 43, 6493–6499.
Wang, X., Shen, Z., Liu, F., Lu, D., Tao, J., Lei, Y., Zhang, Q., Zeng, Y., Xu, H., Wu, Y., Zhang, R., Cao, J., 2018. Saccharides in summer and winter $PM_{2.5}$ over Xi'an, Northwestern China: sources, and yearly variations of biomass burning contribution to $PM_{2.5}$. Atmos. Res. 214, 410–417.
Winklmayr, W., Wang, H.-C., John, W., 1990. Adaptation of the Twomey algorithm to the inversion of cascade impactor data. Aerosol Sci. Technol. 13, 322–331.
Wolfenbarger, J.K., Seinfeld, J.H., 1990. Inversion of aerosol size distribution data. J. Aerosol Sci. 21, 227–247.
Yang, H.-H., Tsai, C.-H., Chao, M.-R., Sua, Y.-L., Chiena, S.-M., 2006. Source identification and size distribution of atmospheric polycyclic aromatic hydrocarbons during rice straw burning period. Atmos. Environ. 40, 1266–1274.
Yttri, K.E., Lund Myhre, C., Eckhardt, S., Fiebig, M., Dye, C., Hirdman, D., Ström, J., Klimont, Z., Stohl, A., 2014. Quantifying black carbon from biomass burning by means of levoglucosan – a one-year time series at the Arctic observatory Zeppelin. Atmos. Chem. Phys. 14, 6427–6442.
Yttri, K.E., Schnelle-Kreis, J., Maenhaut, W., Abbaszade, G., Alves, C., Bjerke, A., Bonnier, N., Bossi, R., Claeys, M., Dye, C., Evtyugina, M., García-Gacio, D., Hillamo, R., Hoffer, A., Hyder, M., Iinuma, Y., Jaffrezo, J.-L., Kasper-Giebl, A., Kiss, G., López-Mahia, P.L., Pio, C., Piot, C., Ramirez-Santa-Cruz, C., Sciare, J., Teinilä, K., Vermeylen, R., Vicente, A., Zimmermann, R., 2015. An intercomparison study of analytical methods used for quantification of levoglucosan in ambient aerosol filter samples. Atmos. Meas. Tech. 8, 125–147.
Zdráhal, Z., Oliveira, J., Vermeylen, R., Claeys, M., Maenhaut, W., 2002. Improved method for quantifying levoglucosan and related monosaccharide anhydrides in atmospheric aerosols and application to samples from urban and tropical locations. Environ. Sci. Technol. 36, 747–753.
Zhang, Y.L., Perron, N., Ciobanu, V.G., Zotter, P., Minguillón, M.C., Wacker, L., Prévôt, A.S.H., Baltensperger, U., Szidat, S., 2012. On the isolation of OC and EC and the optimal strategy of radiocarbon-based source apportionment of carbonaceous aerosols. Atmos. Chem. Phys. 12, 10841–10856.
Zhang, T., Cao, J.J., Chow, J.C., Shen, Z.-X., Ho, K.-F., Sai, S., Ho, H., 2014. Characterization and seasonal variations of levoglucosan in fine particulate matter in Xi'an, China. J. Air Waste Manag. Assoc. 64, 1317–1327.
Zotter, P., Herich, H., Gysel, M., El-Haddad, I., Zhang, Y., Močnik, G., Hüglin, C., Baltensperger, U., Szidat, S., Prévôt, A.S.H., 2017. Evaluation of the absorption Ångström exponents for traffic and wood burning in the Aethalometer-based source apportionment using radiocarbon measurements of ambient aerosol. Atmos. Chem. Phys. 17, 4229–4249.